Bulletin of Mathematical Biology (2009) 71: 906–930
DOI 10.1007/s11538-008-9387-1

ORIGINAL ARTICLE

A Mathematical Model of Liver Cell Aggregation *In Vitro*

J.E.F. Green[a,*,†], S.L. Waters[a,‡], K.M. Shakesheff[b], H.M. Byrne[a]

[a] *Centre for Mathematical Medicine and Biology, School of Mathematical Sciences, University of Nottingham, Nottingham, NG7 2RD, UK*
[b] *Tissue Engineering Group, School of Pharmacy, University of Nottingham, Nottingham, NG7 2RD, UK*

Received: 4 April 2008 / Accepted: 3 December 2008 / Published online: 18 December 2008

Abstract The behavior of mammalian cells within three-dimensional structures is an area of intense biological research and underpins the efforts of tissue engineers to regenerate human tissues for clinical applications. In the particular case of hepatocytes (liver cells), the formation of spheroidal multicellular aggregates has been shown to improve cell viability and functionality compared to traditional monolayer culture techniques. We propose a simple mathematical model for the early stages of this aggregation process, when cell clusters form on the surface of the extracellular matrix (ECM) layer on which they are seeded. We focus on interactions between the cells and the viscoelastic ECM substrate. Governing equations for the cells, culture medium, and ECM are derived using the principles of mass and momentum balance. The model is then reduced to a system of four partial differential equations, which are investigated analytically and numerically. The model predicts that provided cells are seeded at a suitable density, aggregates with clearly defined boundaries and a spatially uniform cell density on the interior will form. While the mechanical properties of the ECM do not appear to have a significant effect, strong cell-ECM interactions can inhibit, or possibly prevent, the formation of aggregates. The paper concludes with a discussion of our key findings and suggestions for future work.

Keywords Cell aggregation · Tissue engineering · Multiphase model

1. Introduction

The liver is the most metabolically complex organ in humans, weighing approximately 1.5 kg, and performing an estimated 500 different functions. Diseases of the liver, in-

*Corresponding author.
E-mail address: egreen@mbi.osu.edu (J.E.F. Green).
†Current address: Mathematical Biosciences Institute, The Ohio State University, Columbus, OH 43210, USA.
‡Current address: Oxford Centre for Industrial and Applied Mathematics, Mathematical Institute, 24-29 St Giles', Oxford, OX1 3LB, UK.

cluding hepatitis and cirrhosis, caused about 46,000 deaths in the USA in 1998 (Centers for Disease Control and Prevention, 2003), and at present there are few successful treatments for such conditions apart from organ transplant. While waiting lists for transplants continue to lengthen, the level of organ donation has remained static (OPTN, 2003; NHS, 2001), so interest is now turning to the development of liver support devices. Passive systems to remove blood toxins accumulated during liver failure (e.g., haemodialysis, haemofiltration, and plasma exchange) have shown disappointing results in terms of patient survival, and so attention has focused on cell-based liver support devices (Jauregui, 2000). The engineering of liver tissue for such devices, for drug testing, and potentially for transplantation, has stimulated new interest in understanding the interactions between the cell populations in the liver, various growth factors, and the extracellular matrix (ECM).

In vivo, under normal physiological conditions, around 80% of liver tissue is composed of hepatocytes (Mitaka, 1998). These epithelial cells perform most of the liver's important functions (Selden et al., 1999), and hence have received the greatest attention from tissue engineers. Hepatocytes cultured *in vitro* often form a monolayer, have a tendency to de-differentiate (lose their ability to function normally) within hours, and die after a few days (Riccalton-Banks et al., 2003; Bhandari et al., 1997). Techniques that have been developed to overcome this problem include coculture with other cell types (such as stellate cells, also found in the liver), culture on polymer scaffolds, and the use of growth factors and cytokines (Bhandari et al., 1997). Some of these techniques result in the hepatocytes forming multicellular spheroids. The structure of the spheroids appears to mimic, in some respects, that of liver tissue *in vivo*; for example, channels resembling bile canaliculi are seen (Abu-Absi et al., 2002). Spheroid culture also results in prolonged expression of liver-specific functions (commonly measured by albumin production (Riccalton-Banks, 2002)) and hepatocyte viability (Richert et al., 2002).

A common procedure for culturing hepatocytes as spheroids involves seeding the freshly isolated cells in culture wells coated with ECM and bathed in a culture medium, which supplies them with nutrients. On suitable substrates, the cells aggregate over a period of approximately one day (Riccalton-Banks, 2002) (Glicklis et al., 2000 also report clustering over a similar timescale for hepatocytes seeded in alginate scaffolds). These aggregates then detach themselves from the surface of the ECM and reorganize to form multicellular spheroids, the diameter of which is around 100–150 μm (Thomas et al., 2005), as we can see from Fig. 1 (compared to a representative cell diameter of 10–30 μm (Higuchi and Tsukamoto, 2004; Glicklis et al., 2000)). The migration of hepatocytes during the early stages of aggregation is described in detail in Powers and Griffith-Cima (1996). They found that only around 6% of observed cells exhibited "classical single-cell locomotion," defined as occurring when a cell translates one body length, without contacting another cell. More frequently, direct cell-cell contact caused by membrane extension facilitated the formation of aggregates. Translation of groups of cells was not quantified in their study, although the authors state that many of the cells translated more than one body length following cell-cell contact.

Hepatocytes are anchorage-dependent cells (Bhandari et al., 1997; Selden et al., 1999), and their interactions with the ECM are believed to be of great importance, both *in vivo* (Bedossa and Paradis, 2003) and *in vitro*. Significantly, experiments have shown that the material properties of the ECM affects the morphology of the cells, the likelihood of aggregation, and the ability of the cells to sustain liver specific functions (Moghe et al., 1996; Powers et al., 1997). Tissue engineers employ a wide variety of ECM types; often these

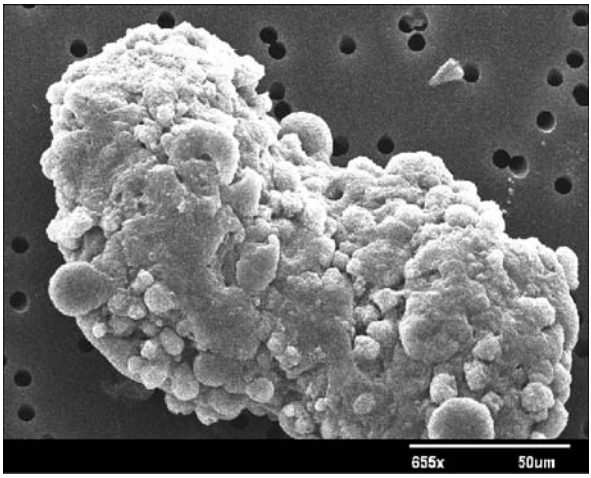

Fig. 1 Scanning electron micrograph of a multicellular liver spheroid (courtesy of L. Riccalton-Banks).

are artificial substrates such as tissue culture plastic or polylactic acid; however, unlike the ECM *in vivo*, such substrates lack specific recognition groups for cells. Matrix proteins such as fibronectin can be employed to modify such surfaces, and provide a more favorable environment for attachment (see Whitaker, 2003, Chap. 5). Another approach is to culture the cells on natural ECM components, such as Matrigel or in a collagen sandwich (Richert et al., 2002). In addition to cell-ECM interactions, cell-cell contacts appear to play a significant role, and studies have shown that spheroid formation is inhibited if the initial cell plating density is too high or too low (Peshwa et al., 1994, 1996). Cell-cell interactions are also important in maintaining the viability and functionality of the hepatocytes (Moghe et al., 1997).

Previous modeling work on this problem appears limited. Glicklis et al. (2004) assumed the diameter of individual liver cell spheroids undergoes logistic growth, and determined the values of the relevant parameters by fitting to experimental data. They then used this solution to determine the rate of albumin production. By contrast, cell aggregation in the slime mold *Dictyostelium discoideum* has been extensively studied by theoreticians. In this organism, when nutrients are scarce, aggregation is stimulated by gradients of a cell-derived chemical (cAMP) (Vasiev and Weijer, 2003). This phenomenon provided the motivation for the development of the best known model for chemotactic cell movement, due to Keller and Segel (1970, 1971). Although chemotaxis is also a potential mechanism for hepatocyte aggregation (see Section 6), for simplicity we do not explicitly consider chemical signals in this paper. Instead, we base our approach on the ideas of Murray and co-workers (Murray, 1993), who developed continuum models which include the effects of cell interactions with the ECM. They propose a general equation for the evolution of the cell density, in which cell movement involves a combination of random motion, chemotaxis and advection with the ECM. The principles of mass and momentum balance are used to derive equations for the density and deformations of the ECM. Models of this type offer enormous scope for generating many different types of spatial patterns, and have been studied in connection with a wide variety of systems, including limb-bud

formation, wound healing, and cancer. An alternative approach that has been used to describe the formation of vascular networks *in vitro*, involves coupling a mass conservation equation for the cell density to a Burgers-type equation for the cell velocity (Kowalczyk et al., 2004 and references therein), rather than simply prescribing the cell flux as a function of cell density and ECM displacement as in Murray (1993). The velocity equation also contains a Keller–Segel type term describing chemotaxis, which is in turned coupled to a reaction diffusion equation for the chemoattractant in the conventional way.

As the review above suggests, there is increasing interest in developing mathematical models which describe interactions between cells and other constituents of their environment, such as extracellular fluid (Breward et al., 2002), ECM (Jackson and Byrne, 2002; Lemon et al., 2006) and other cell populations, e.g., macrophages (Owen et al., 2004). Multiphase models, in which the different components are treated as distinct phases, represent a natural framework within which to study such systems. The principles of mass and momentum conservation are applied to each phase, and the physical properties of the different phases, and the interaction forces between them, specified by constitutive relations. We use this approach here to study the early stages of liver cell spheroid formation.

The paper is organized as follows: in Section 2, we derive the governing equations and show how they may be reduced to a system of four coupled PDEs; in Section 3, we apply linear stability analysis to the model, to determine the parameter regimes in which we can expect to observe aggregation, while in Section 4, we consider behavior for long times. This is followed in Section 5 by numerical simulations of the governing equations. (A weakly nonlinear analysis of a modified version of the model is presented in Appendix A.) The paper concludes with a discussion in Section 6, summarizing our main results, and suggesting possible directions for future work.

2. Model formulation

We consider an *in vitro* population of cells (hepatocytes) bathed in culture medium, which we treat as a two-phase mixture. The cells adhere to a deformable layer of ECM which occupies the base of the culture well (see Fig. 2). For simplicity, a one-dimensional slab geometry is adopted, we neglect the effects of chemotaxis and assume that the cells are nutrient-rich. The model is then developed, in Section 2.1, as a series of mass and momentum balances for the cells, culture medium and ECM. We close the model in Section 2.2 by introducing appropriate constitutive laws for the mechanical properties of each of the three species. Finally, interaction forces and suitable boundary and initial conditions are specified in Section 2.3.

2.1. Governing equations

We assume the culture well occupies the region $-L \leq x \leq L$. We denote the local volume fractions of the cells and culture medium by $n(x,t)$ and $w(x,t)$ and their horizontal velocities by $v_n(x,t)$ and $v_w(x,t)$. The ECM density and displacement are denoted by $\rho(x,t)$ and $s(x,t)$, respectively. For simplicity, we consider only small ECM displacements, so that linear theory is valid, and the ECM velocity is given by $\partial s/\partial t$.

In the cell and culture medium mixture, we assume there are no voids, so

$$n + w = 1. \tag{1}$$

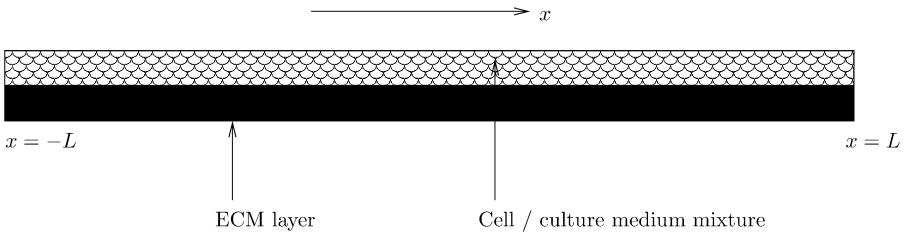

Fig. 2 Definition sketch.

As cells consist predominantly of water, we assume that cells and culture medium have an equal, constant density ($\equiv 1$, without loss of generality) and exclude this factor from the relevant mass balance equations. Data on the rates of proliferation and death of hepatocytes in culture are limited. Enat et al. (1984) report that the ratio of the number of cells on day 7 of culture compared to that on day 1 is 1.0–2.9 (depending on the type of ECM and culture medium used), while Thomas et al. (2006) found around 10% of cells died between 24 and 48 hours in culture. Since the timescale of interest for aggregation is around 1 day, this suggests that cell proliferation is not the main cause of cluster formation. For simplicity, we thus neglect hepatocyte proliferation and death, and likewise production and degradation of ECM, and hence obtain the following mass conservation equations for n, w, and ρ:

$$\frac{\partial n}{\partial t} + \frac{\partial}{\partial x}(n v_n) = 0, \tag{2a}$$

$$\frac{\partial w}{\partial t} + \frac{\partial}{\partial x}(w v_w) = 0, \tag{2b}$$

$$\frac{\partial \rho}{\partial t} + \frac{\partial}{\partial x}\left(\rho \frac{\partial s}{\partial t}\right) = 0. \tag{2c}$$

We denote by σ_n, σ_w, and σ_ρ the Cauchy stresses in the cells, culture medium, and ECM. Neglecting inertial effects, the momentum balance in each phase is given by:

$$\frac{\partial}{\partial x}(n\sigma_n) + F_n = 0, \tag{3a}$$

$$\frac{\partial}{\partial x}(w\sigma_w) + F_w = 0, \tag{3b}$$

$$\frac{\partial \sigma_\rho}{\partial x} + F_\rho = 0, \tag{3c}$$

where F_n, F_w, and F_ρ represent the net sources of momentum in each phase, the precise forms of which are discussed in Section 2.2.

2.2. *Constitutive relations*

We model the culture medium as an inviscid fluid for which

$$\sigma_w = -p, \tag{4}$$

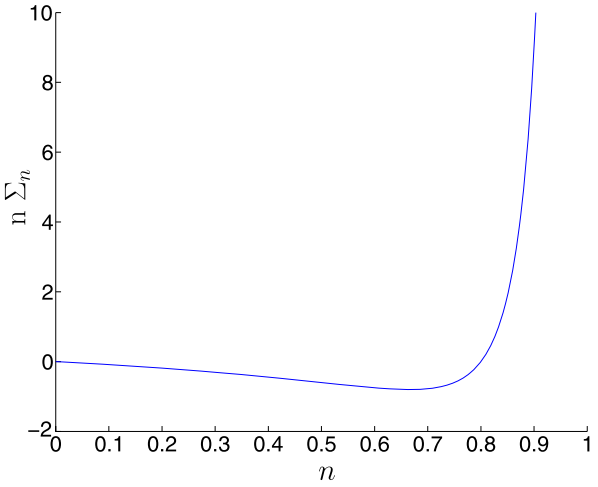

Fig. 3 $n\Sigma_n$ against n ($n^* = 0.8$, $\Gamma_1 = 1$).

where p is the fluid pressure.

We model the cells as an incompressible viscous fluid, with constant viscosity μ_n. The viscous effects are intended to capture the tendency of cells to align and match their velocities with the local average cell velocity (Babak et al., 2004). In the context of liver cell aggregation, the viscous term represents migration of hepatocytes as coupled pairs or groups (Powers and Griffith-Cima, 1996). Obviously, cells differ from viscous fluids in that they are able to generate forces in response to cues from their environment, such as variations in the local cell density. We assume these forces manifest themselves in the cellular phase as an additional pressure term, Σ_n Thus, following Breward et al. (2002), we write

$$\sigma_n = -p - \Sigma_n + 2\mu_n \frac{\partial v_n}{\partial x}, \tag{5}$$

where

$$\Sigma_n = \Gamma_1 \frac{(n - n^*)}{(1-n)^2}. \tag{6}$$

In the above, the tension constant, Γ_1, describes the cells' affinity for the *close-packing* volume fraction $n^* \in (0, 1)$. We note from Eq. (3a) that it is, in fact, $n\Sigma_n$ that is key for cell movement. This function has a single turning point at $n = n_c = n^*/(2 - n^*)$. For $n < n_c$, the effect is for cells to move up gradients of n (i.e., cell-cell interactions are attractive), and conversely for $n > n_c$. A graph of $n\Sigma_n(n)$ is presented in Fig. 3.

We model the ECM as an isotropic, viscoelastic material, over which the cells move (see Fig. 2). In general, mechanochemical models are sensitive to the particular constitutive laws adopted (Byrne and Chaplain, 1996). However, in the absence of appropriate experimental data, we use the Voigt model of viscoelasticity (see, e.g., Gracheva and Othmer, 2004) to describe the mechanical properties of the ECM. This model exhibits

viscous behavior over short timescales, and elastic behavior at long times. The stress and displacement in the ECM are related as follows:

$$\sigma_\rho = \frac{\partial}{\partial x}\left(\mu_E \frac{\partial s}{\partial t} + E' s\right), \tag{7}$$

where μ_E and E' are the viscous and elastic constants for the material. (In fact, μ_E is the sum of the bulk and shear viscosities of the material, and E' is related to the Young's modulus E and Poisson ratio ν by $E' = E(1-2\nu)(1-\nu)/(1+\nu)$ (Murray, 1993)).

Turning to the momentum source terms, F_n, F_w, and F_ρ, we assume that the culture medium and ECM exert drag forces on the cells (and *vice versa*), but neglect any drag between the ECM and the culture medium. Our choice of cell-ECM interaction term thus differs from that of Murray (1993), where a "tethering" force proportional to the ECM displacement, s, is used. We denote by k_{nw} and $k_{n\rho}$ the cell-culture medium and cell-ECM drag coefficients and, following Breward et al. (2002), we fix $k_{nw} = k_1 nw$ and $k_{n\rho} = k_2 n\rho$ for nonnegative constants k_1 and k_2. Consequently, there is no drag if either of the two species concerned is not present.

Combining the above information, we write

$$F_n = -k_2 n\rho\left(v_n - \frac{\partial s}{\partial t}\right) - k_1 nw(v_n - v_w) + p\frac{\partial n}{\partial x}, \tag{8a}$$

$$F_w = -k_1 nw(v_w - v_n) + p\frac{\partial w}{\partial x}, \tag{8b}$$

$$F_\rho = k_2 n\rho\left(v_n - \frac{\partial s}{\partial t}\right). \tag{8c}$$

The last term in Eqs. (8a) and (8b) represents the contribution of interfacial forces, assuming surface tension effects are negligible (see Drew and Segel, 1971; Drew, 1983 for a detailed derivation).

2.3. Initial and boundary conditions

The model comprises Eqs. (2)–(3), together with the constitutive relations (4)–(8). We close the model by specifying appropriate boundary and initial conditions. The initial distribution of cells is given by

$$n(x,0) = n_0(x). \tag{9}$$

Initially, the ECM layer is taken to be undeformed and spatially uniform with constant density ρ_0, so that

$$\rho(x,0) = \rho_0, \qquad s(x,0) = 0. \tag{10}$$

We assume that the system is symmetric about $x = 0$; accordingly, we restrict attention to $0 \le x \le L$ and impose

$$s(0,t) = v_n(0,t) = v_w(0,t) = 0. \tag{11}$$

The ECM is taken to be pinned at the edge of the culture well, so the displacement is zero at $x = L$, i.e.,

$$s(L,t) = 0. \tag{12}$$

We also assume there is no flux of cells or water out of the culture well, so

$$v_n(L,t) = v_w(L,t) = 0. \tag{13}$$

2.4. Model simplification

The model developed in Sections 2.1–2.3 can be reduced to coupled PDEs for n, ρ, v_n, and s. This allows us to focus on the four physical quantities with which we are most concerned. Although we eliminate the variables w, v_w, and p, these quantities may be determined, if required, using expressions derived below.

Adopting the functional forms introduced in Section 2.2, the momentum balance Eqs. (3) become:

$$\frac{\partial}{\partial x}\left(2\mu_n n\frac{\partial v_n}{\partial x} - n\Sigma_n\right) - n\frac{\partial p}{\partial x} - k_2 n\rho\left(v_n - \frac{\partial s}{\partial t}\right) - k_1 n w(v_n - v_w) = 0, \tag{14a}$$

$$w\frac{\partial p}{\partial x} + k_1 n w(v_w - v_n) = 0, \tag{14b}$$

$$\frac{\partial^2}{\partial x^2}\left(\mu_E\frac{\partial s}{\partial t} + E's\right) + k_2 n\rho\left(v_n - \frac{\partial s}{\partial t}\right) = 0. \tag{14c}$$

Summing Eqs. (2) leads to the incompressibility relation:

$$\frac{\partial}{\partial x}(nv_n + wv_w) = 0, \tag{15}$$

which following integration and imposition of (11) yields

$$v_w = \frac{-nv_n}{w} \tag{16}$$

(assuming $w \neq 0$). We combine Eqs. (1) and (16) to eliminate w and v_w in (14b) and deduce that

$$\frac{\partial p}{\partial x} = \frac{k_1 n}{(1-n)}v_n. \tag{17}$$

Using (17) in Eq. (14a) gives

$$\frac{k_1 n}{(1-n)}v_n + k_2 n\rho\left(v_n - \frac{\partial s}{\partial t}\right) + \frac{\partial}{\partial x}(n\Sigma_n) - 2\mu_n\frac{\partial}{\partial x}\left(n\frac{\partial v_n}{\partial x}\right) = 0. \tag{18}$$

The reduced model comprises Eqs. (2a), (2c), (14c), and (18) for n, ρ, s, and v_n, respectively, together with the initial and boundary conditions specified by Eqs. (9)–(10), (11)–(13).

Table 1 Summary of dimensional parameter values and the corresponding references

Parameter	Symbol	Units	Value	Source
Aggregate lengthscale	λ	m	10^{-4}	Thomas et al. (2005)
Domain half-length	L	m	10^{-2}	Measured
Cell close-packing volume fraction	n^*	none	0.8	Powers et al. (2002)
Aggregation timescale	T^*	s	10^5	Riccalton-Banks (2002)
ECM density	ρ_0	kg m^{-3}	0.5–8	Namy et al. (2004) and refs. therein
Cell-water drag[a]	k_1	kg m^{-3} s^{-1}	10^7–10^{11}	Swabb et al. (1974), Lubkin and Jackson (2002)
Cell-ECM drag	k_2	kg m^{-3} s^{-1}	no data	N/A
Tension constant	Γ_1	kg m^{-1} s^{-2}	no data	N/A
Cell viscosity[b]	μ_n	s^{-1}	10^4–10^6	Forgacs et al. (1998), Lubkin and Jackson (2002)
ECM viscosity (collagen)	μ_E	kg m^{-1} s^{-1}	10^5	Velegol and Lanni (2001)
ECM shear modulus (collagen)	E'	Pa	10^0–10^1	Velegol and Lanni (2001)
ECM viscosity (PLA)	μ_E	kg m^{-1} s^{-1}	10^5–10^8	Namy et al. (2004), Chen et al. (2003), Gunatillake and Adhikari (2003)
ECM shear modulus (PLA)	E'	Pa	10^6–10^9	Namy et al. (2004), Chen et al. (2003), Gunatillake and Adhikari (2003)

[a]Measurements in Swabb et al. (1974) relate to hepatoma

[b]Measurements in Forgacs et al. (1998) are for spherical aggregates of embryonic chick liver cells

2.5. *Parameters*

Here, we estimate the physical parameters in the model. The associated lengthscales range from the diameter of a cell ($\sim$10 μm) to that of a liver cell spheroid ($\lambda \sim 150$ μm) to that of the culture well ($L \sim 1$ cm). Our interest in aggregation prompts us to use λ to fix a typical lengthscale. Our timescale T^* is related to the time for aggregation to occur ($T^* \sim 1$ day, Riccalton-Banks, 2002; Thomas et al., 2005). We estimate the packing density to be $n^* = 0.8$ (see Powers et al., 2002).

The types of ECM used in liver tissue engineering include collagen gels and polylactic acid (PLA); for the former, $\mu_E \sim 10^5$ Pa and $E' \sim 10^0$–10^1 Pa (Velegol and Lanni, 2001), while for the latter, $\mu_E \sim 10^5$–10^8 Pa and $E' \sim 10^6$–10^9 Pa (Chen et al., 2003; Gunatillake and Adhikari, 2003; Namy et al., 2004). We thus consider a range of values for these parameters. The values of the cell viscosity μ_n, cell-culture medium drag constant k_1 and the initial ECM density ρ_0 are estimated from similar experiments reported in the literature. The parameter values and supporting references are summarized in Table 1.

At present, values for the cell-ECM drag constant, k_2, and the tension constant Γ_1 cannot be determined from the literature and so must be estimated. We assume that the drag force between the cells and ECM is stronger than that between the cells and culture medium, and hence take $k_2\rho_0 \geq k_1$. We estimate the timescale for aggregation in the absence of drag effects to be $T^* \sim 2\mu_n/\Gamma_1$, and use this to estimate Γ_1. Given $T^* \sim 10^5$ s and using the range for μ_n stated in Table 1, we predict $\Gamma_1 \sim 10^{-1}$–10^1 kg m^{-1} s^{-2}.

2.6. Dimensionless governing equations

We nondimensionalize as follows

$$\tilde{x} = \frac{x}{\lambda}, \qquad \tilde{t} = \frac{\Gamma_1 t}{2\mu_n}, \qquad \tilde{\rho} = \frac{\rho}{\rho_0}, \qquad \tilde{v}_n = \frac{2\mu_n v_n}{\Gamma_1 \lambda}, \qquad \tilde{s} = \frac{\mu_E s}{2\lambda\mu_n},$$

where tildes denote dimensionless quantities. Note that in the above, we have adopted the timescale $T^* = 2\mu_n/\Gamma_1$, which gives a balance between the cell viscosity and cell-generated forces. The dimensionless governing equations are then (dropping tildes for convenience):

$$\frac{\partial n}{\partial t} + \frac{\partial}{\partial x}(n v_n) = 0, \tag{19}$$

$$\frac{\partial \rho}{\partial t} + \frac{1}{\hat{\mu}}\frac{\partial}{\partial x}\left(\rho \frac{\partial s}{\partial t}\right) = 0, \tag{20}$$

$$\frac{\hat{k}_1 n}{(1-n)} v_n + \hat{k}_2 n\rho\left(v_n - \frac{1}{\hat{\mu}}\frac{\partial s}{\partial t}\right) + \frac{\partial}{\partial x}\left(\frac{n(n-n^*)}{(1-n)^2}\right) - \frac{\partial}{\partial x}\left(n\frac{\partial v_n}{\partial x}\right) = 0, \tag{21}$$

$$-\hat{k}_2 n\rho\left(v_n - \frac{1}{\hat{\mu}}\frac{\partial s}{\partial t}\right) = \frac{\partial^2}{\partial x^2}\left(\frac{\partial s}{\partial t} + \tau s\right), \tag{22}$$

where

$$\hat{k}_1 = \frac{k_1\lambda^2}{2\mu_n}, \qquad \hat{k}_2 = \frac{k_2\lambda^2\rho_0}{2\mu_n}, \qquad \hat{\mu} = \frac{\mu_E}{2\mu_n}, \qquad \tau = \frac{2\mu_n E'}{\mu_E \Gamma_1}, \qquad \epsilon = \frac{\lambda}{L}.$$

The parameters $\hat{k}_1$ and $\hat{k}_2$ are the ratios of cell-culture medium and cell-ECM drag to viscous forces; $\hat{\mu}$ is the ratio of the ECM and cell viscosities; and τ is the ratio of the aggregation timescale to the ECM relaxation time, $T_R = \mu_E/E'$ (i.e. T_R is the time taken for an ECM deformation to decay by a factor e^{-1} in the absence of external forces).

The initial conditions are now applied over the large domain $[0, \epsilon^{-1}]$ (given the length-scales stated in Section 2.5, $\epsilon^{-1} \approx 50$). They give

$$n(x,0) = n_0(x), \qquad \rho(x,0) = 1, \qquad s(x,0) = 0, \tag{23}$$

while the boundary conditions for v_n and s become

$$v_n(0,t) = v_n\left(\epsilon^{-1}, t\right) = 0, \qquad s(0,t) = s\left(\epsilon^{-1}, t\right) = 0. \tag{24}$$

3. Linear stability analysis

Equations (19)–(22), together with their associated boundary conditions (24) have a spatially homogeneous steady state solution for which $(n, \rho, v_n, s) = (n_0, 1, 0, 0)$ with $0 < n_0 < 1$ constant. This solution approximates the conditions immediately after the liver cells have been seeded in the culture wells. We examine the linear stability of this

steady state to determine parameter ranges in which aggregation may occur. We consider perturbations of the form

$$n = n_0 + \hat{n}e^{iqx+\omega t}, \qquad \rho = 1 + \hat{\rho}e^{iqx+\omega t},$$
$$v_n = \hat{v}_n e^{iqx+\omega t}, \qquad s = \hat{s}e^{iqx+\omega t}, \tag{25}$$

where the real part is to be understood, and $|\hat{n}|$, $|\hat{\rho}|$, $|\hat{v}_n|$, and $|\hat{s}| \ll 1$. Here, q is the wavenumber of a given perturbation and $\omega = \omega(q)$ is the corresponding growth rate. The no-flux boundary conditions impose the constraint $q = m\pi\epsilon$, where m is an integer.

For a given q, if there exists an $\omega(q)$ for which $\mathcal{R}(\omega) > 0$ (< 0), then the steady state is linearly unstable (stable) with respect to perturbations of the form (25). We expect aggregation to occur in parameter regimes for which the steady state is linearly unstable.

We substitute (25) into Eqs. (19)–(22), linearize, and obtain the following dispersion relation for $\omega(q)$:

$$A(q^2)\omega^2 + B(q^2)\omega + C(q^2) = 0, \tag{26}$$

where

$$A = \hat{k}_2 n_0\left(\frac{\hat{k}_1}{(1-n_0)} + q^2\right) + q^2\hat{\mu}\left(\frac{\hat{k}_1}{(1-n_0)} + \hat{k}_2 + q^2\right),$$
$$B = q^2\hat{\mu}\tau\left(\frac{\hat{k}_1}{(1-n_0)} + \hat{k}_2 + q^2\right) + q^2\beta(n_0)\frac{(\hat{k}_2 n_0 + q^2\hat{\mu})}{(1-n_0)^3},$$
$$C = \frac{q^4\tau\hat{\mu}\beta(n_0)}{(1-n_0)^3},$$

and $\beta(n_0) = 2n_0 - n^*(1+n_0)$. With the exception of $\beta(n_0)$, all model parameters are positive. Hence, $A > 0$ and the behavior of (26) depends, via $\beta(n_0)$, on the signs of B and C. If $\beta(n_0) > 0$, then $B, C > 0$ and the system is linearly stable ($\mathcal{R}(\omega(q)) < 0$). If $\beta(n_0) < 0$, then $C < 0$ and the system is unstable (the roots of (26) are real and of opposite sign).

The above analysis suggests that the stability of the system depends only on the initial cell seeding density, n_0. In particular, if $n_0 > n_c = n^*/(2-n^*)$, then $\beta(n_0) > 0$, the cell-cell interaction force is repulsive and the spatially uniform steady state is locally stable. If instead $n_0 < n_c$, then $\beta(n_0) < 0$ and the steady state is unstable, the cells moving to achieve their preferred density. We note from Eq. (26) that ω is bounded (but may be positive) as $q \to \infty$, since the highest power of q is the same in A, B, and C. As a result, modes with large wavenumber grow at almost equal rates. In order to distinguish between these modes, the impact of nonlinear effects must be investigated. We use numerical methods to do this in Section 5, and illustrate how analytical methods may be used in Appendix A, where we perform a weakly nonlinear analysis of a modified version of the model. First, however, we consider the long-time dynamics.

4. Long-time behavior

We consider the long-time behavior of the model, by adopting the timescale $t = \delta^{-1}T$ (where $\delta \ll 1$). This has the effect of eliminating the time derivative term in Eq. (19)

at leading order, and upon integrating and applying the boundary conditions, we find $nv_n = 0$. At leading order, Eq. (22) then becomes

$$\frac{\partial^2 s}{\partial x^2} = 0.$$

On integrating and applying the boundary conditions, we find $s = 0$, and thus Eq. (20) (which is unchanged by the rescaling at leading order) implies ρ is an arbitrary function of x (which will depend on the behavior at earlier times). Assuming $n \neq 0$ (otherwise Eq. (21) is trivially satisfied), we find at leading order:

$$\frac{\partial}{\partial x}\left(\frac{n(n-n^*)}{(1-n)^2}\right) = 0. \tag{27}$$

We observe that two types of behavior may satisfy (27). The first possibility is that $n = const.$, but as we have seen from Section 3, the spatially uniform state is unstable for $n < n_c$, so we would not expect to observe this behavior if at any time $n < n_c$ anywhere in the domain. The second possibility is that n is piecewise constant, taking the values 0 and n^* in different regions. This suggests that at long times, we may tend toward a situation in which there are aggregates within which the cells achieve their close-packing density, alternating with regions devoid of cells.

Since the role of cell-ECM adhesion is of particular interest, we also briefly consider the long-time behavior in the limit of large $\hat{k}_2$, for which cell-ECM drag is strong. Taking $\hat{k}_2 \gg 1$, we introduce the long timescale $t = \hat{k}_2 T$ and the slow cell velocity scale $v_n = V/\hat{k}_2$. Under these rescalings, Eqs. (19) and (20) are unchanged at leading order, while Eqs. (21) and (22) become

$$n\rho\left(V - \frac{\partial s}{\partial T}\right) + \frac{\partial}{\partial x}\left(\frac{n(n-n^*)}{(1-n)^2}\right) = 0, \tag{28}$$

$$-n\rho\left(V - \frac{\partial s}{\partial T}\right) = \hat{\mu}\tau\frac{\partial^2 s}{\partial x^2}. \tag{29}$$

Combining Eqs. (28) and (19) gives the following nonlinear diffusion equation for n

$$\frac{\partial n}{\partial T} + \frac{\partial}{\partial x}\left(n\frac{\partial s}{\partial t} - \frac{1}{\rho}\frac{\partial}{\partial x}\left(\frac{n(n-n^*)}{(1-n)^2}\right)\right) = 0. \tag{30}$$

We note from (28) that V includes a term representing advection of the cells with the ECM as it is deformed. The form of this term is identical to that prescribed by Murray (1993), though we have derived it here from a momentum balance. We also note that Eq. (30) is ill-posed when $n < n_c = n^*/(2 - n^*)$; this would suggest the formation of localized regions of high or low cell density (Oliver et al., 2005). This is indeed what is seen numerically, with the formation of smaller aggregates for larger $\hat{k}_2$ (see, e.g., Fig. 7). (We remark that although the above equation is ill-posed, retention of a small viscous term in the full system renders it well posed.)

The type of solution described in this section, in which the value of n changes abruptly in space, is similar to those involving the formation of shocks described in Byrne and Preziosi (2003) for a two-phase model of tumor growth (in which the cell viscosity is

neglected). While the above analysis provides useful qualitative information on the long-time behavior of our model, it does not tell us the positions at which n "jumps," and hence the number of aggregates we can expect to observe. This will depend on the initial conditions, and the evolution of the model over $O(1)$ timescales, and must hence be investigated numerically. This is undertaken in the following section.

5. Numerical simulations

5.1. Numerical methods

The governing Eqs. (19)–(22) were discretized using second-order accurate finite difference methods, and simulations were performed using MATLAB as follows. Firstly, given the initial conditions for n, ρ, and s, we solved the discretized versions of Eqs. (21) and (22) by a simple matrix inversion to obtain v_n and $\partial s/\partial t$. These values were then used to update n and ρ at the next timestep, using Eqs. (19) and (20). The latter two equations are solved using a Crank–Nicholson type method (Strikwerda, 1989) (with the relevant velocities evaluated at the current timestep). We found it convenient to include a small stabilizing diffusion term in Eq. (19) (with diffusion coefficient $D = 10^{-4}$) to reduce the number of points in the spatial discretization needed to obtain satisfactorily smooth solutions. The solution for s was then updated using the values of $\partial s/\partial t$ found in the initial step, using a method which is first-order accurate in time. The updated solutions for n, ρ, and s were then used to determine v_n and $\partial s/\partial t$ at the new timestep, and the process described above was repeated until the desired end time was reached. The growth rates of the numerical solutions for early times were verified against those predicted by the linear stability analysis.

For convenience, the domain is truncated to $0 \leq x \leq 10$ (numerical experiments with longer domains give the same qualitative results; results not presented). For the simulations presented in the following section, a timestep $\Delta t = 0.01$ and $N = 2001$ grid points were used.

5.2. Numerical results

Unless otherwise stated, henceforth, we fix $n^* = 0.8$ and $\hat{k}_1 = \hat{k}_2 = \tau = \hat{\mu} = 1$, which is consistent with the ranges suggested in Section 2.5. For simplicity, we begin by setting $n(x, 0) = 0.5 + 0.01 \cos 0.6\pi x$ (other initial conditions will be considered later). The corresponding numerical simulations show the formation of aggregates which have sharply defined edges (except for those where the edge of the aggregate coincides with the edge of the domain), and uniform cell density (equal to $n^* = 0.8$) on the interior (Fig. 4). This agrees with the predictions of the long-time behavior in Section 4. Note that in this simulation, the number of aggregates corresponds to the number of peaks in the initial condition.

During the early stages of aggregation, cell movement is slow (in Fig. 5 $|v_n| < 0.05$ for $0 \leq t \leq 2$). Between $t = 2$ and $t = 4$, the cell velocity increases considerably and aggregation proceeds relatively quickly (Fig. 5a). For $t \geq 5$, we note that we tend to observe $v_n = 0$ within aggregates (compare Figs. 4 and 5b); elsewhere $v_n \neq 0$, with the few remaining cells moving toward the nearest cluster. As the cells begin to aggregate, the

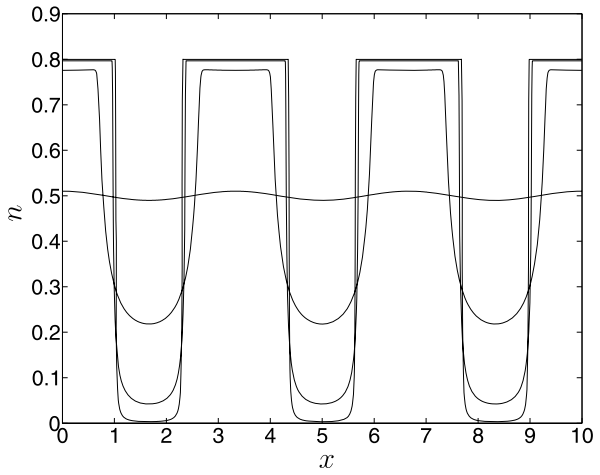

Fig. 4 Numerical solution for cell volume fraction, n, at times $t = 0, 5, 10, 15$ ($\hat{k}_1 = \hat{k}_2 = \hat{\mu} = \tau = 1$).

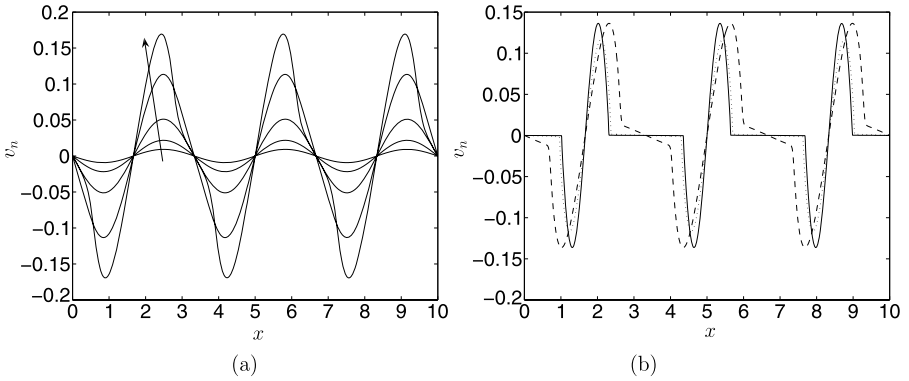

Fig. 5 Numerical solution for cell velocity, v_n at: (a) $t = 0, 1, 2, 3, 4$ (arrow indicates increasing time); (b) $t = 5$ (dashed), $t = 10$ (dotted) and $t = 15$ (solid). Parameter values as for Fig. 4.

ECM is at first pulled along with them, so that its density is increased within the growing aggregates (Fig. 6a). At later times, when most of the cells have stopped moving, elastic forces begin to reduce the deformation of the ECM (Fig. 6b) until its density becomes spatially uniform once again.

We now investigate the effect of varying key model parameters on the behavior of the system. The parameters over which tissue engineers have most control are: the strength of cell-ECM adhesion $\hat{k}_2$, which can be changed, for example, by surface modification of the substrate with various proteins; the physical properties of the ECM, represented by $\hat{\mu}$ and τ; the degree of drag between the cells and the culture medium $\hat{k}_1$, which will depend on the viscosity of the culture medium; and the initial cell seeding density, $n(x, 0)$.

Increasing the cell-ECM drag parameter $\hat{k}_2$ has two effects on cell aggregation. It increases the number of aggregates formed (with a corresponding reduction in their size)

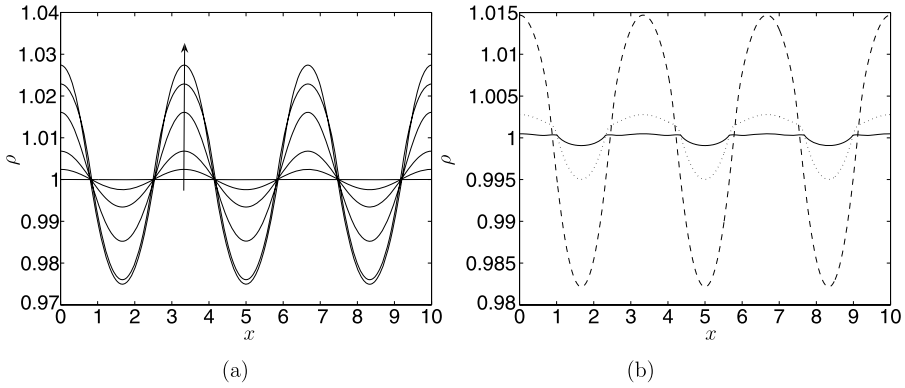

Fig. 6 (a) Numerical solution for ECM density, ρ, at $t = 0, 1, 2, 3, 4, 5$ (arrow indicates increasing time); (b) $t = 6$ (dashed), $t = 10$ (dotted) and $t = 15$ (solid). Parameter values as for Fig. 4.

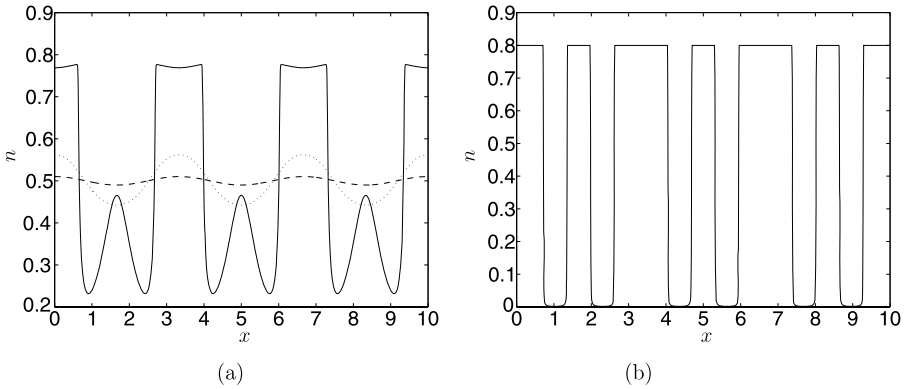

Fig. 7 (a) Numerical solution for cell volume fraction, n, at $t = 0$ (dashed), $t = 5$ (dotted) and $t = 10$ (solid); (b) $t = 20$. Parameter values as for Fig. 4, except $\hat{k}_2 = 10$.

and reduces the cells' speed. Taking the same initial condition as for Fig. 4, and setting $\hat{k}_2 = 10$ (with other parameters unchanged), we see that initially four aggregates begin to form as before. However, at later times, additional aggregates begin to form in the spaces between the original ones (Fig. 7a). By $t = 20$, 7 aggregates have formed (Fig. 7b). A further increase to $\hat{k}_2 = 30$ produces a further increase in the number of aggregates to 9. In each case, there is a corresponding reduction in $|v_n|$ (results not presented). A similar effect occurs when the cell-culture medium drag parameter $\hat{k}_1$ is increased. Setting $\hat{k}_1 = 5$ (with other parameter values and initial conditions as for Fig. 4) results in the formation of 7 aggregates; while for $\hat{k}_1 = 10$ this number increases to 9 (results not presented).

Repeated simulations suggest that altering the ECM compliance (by changing $\hat{\mu}$ and τ) does not affect the qualitative nature of the cells' aggregation (results not presented). We do, however, see predictable changes in the ECM, with density variations almost eliminated for stiff substrates (large $\hat{\mu}$, τ) and increased deformation with increased compliance.

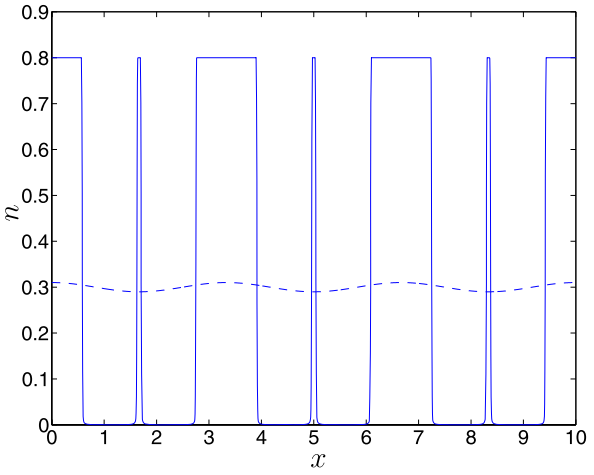

Fig. 8 Numerical solution for n at $t = 0$ (dotted) and $t = 20$ (solid). Reduced cell seeding density $n(x, 0) = 0.3 + 0.01 \cos 0.6\pi x$. Parameter values as for Fig. 4.

The final factor we wish to consider is the effect of the initial cell seeding density, $n(x, 0)$, on the formation of aggregates. We begin by setting the parameter values as for Fig. 4, and rerunning the simulation for the initial condition $n(x, 0) = 0.6 + 0.01 \cos 0.6\pi x$. The result is that the same number of aggregates are formed as before, but the aggregates are larger, as there are more cells in the system (results not shown). If we continue to increase the cell seeding density, so that the initial condition has $n(x, 0) > n_c = 2/3$ (for $n^* = 0.8$), then the cells spread so that n becomes spatially uniform, as predicted by the linear stability analysis in Section 3. Still using the same parameter values, but with $n(x, 0) = 0.3 + 0.01 \cos 0.6\pi x$, we find that seven, rather than four, aggregates form (Fig. 8). The additional aggregates (which form between the four peaks of the initial condition) are extremely narrow.

A further question of interest is: How does the initial distribution of the cells affect the final number and size of aggregates? Our previous simulations, using sinusoidal initial conditions, impose a degree of symmetry on the solution which is unrealistic (though using these initial conditions is useful in identifying the effects of changing parameter values). In order to determine if the system dynamics naturally favor the formation of aggregates of a particular size, we considered the effect of using random initial conditions. These were obtained by taking the Fourier transform of a vector of length N, the entries of which were uniformly distributed on the interval [0, 1]. The higher-wavenumber ($q > 20$) modes were then eliminated, and the inverse transform of the real part of the resulting vector was then normalized to give a perturbation with amplitude 0.01. We then set $n(x, 0) = const. + f(x)$, where $f(x)$ is the perturbation obtained as just described. Taking the parameter values as for Fig. 4, with the constant part of the initial condition set at 0.5, we performed five simulations for different realizations of the initial conditions. These resulted in the formation of the following numbers of aggregates: 7 (twice), 9 (twice), 11 (once). The average lengths of the aggregates (defined as regions where $n > 0.79$) were in the range 0.55 to 0.87. These results are broadly similar to those obtained with dif-

ferent random initial conditions, reported in Green (2006). This suggests that the initial conditions have only a limited influence on the number of aggregates that form.

6. Discussion

In this paper, we have developed a new model of liver cell aggregation *in vitro*. The mass and momentum balances for the cell phase are similar to those of Kowalczyk et al. (2004), except that we neglect "inertia" terms (which represent directional persistence). In addition, we have used a two-phase modeling framework to couple the motion of the cells and culture medium, postulating constitutive laws for the interaction forces between phases. Our simulations show the formation of "aggregates" with clearly defined outer boundaries, and spatially uniform cell density in the interior. This is in good qualitative agreement with images of aggregates cultured *in vitro* (Riccalton-Banks et al., 2003; Thomas et al., 2005).

It is well known that both the strength of cell-ECM adhesion and the material properties of the ECM contribute significantly to cell mobility (Powers and Griffith-Cima, 1996; Thomas and DiMilla, 2000). Our results show that strong cell-ECM adhesion results in the formation of larger numbers of smaller aggregates, and increases the time taken for aggregates to form. Our results agree with experimental findings reported in Powers and Griffith-Cima (1996), that strong cell-substrate adhesion inhibits migration, and are consistent with the hypothesis that aggregates do not form when cell-ECM adhesions are stronger than cell contractile forces. When cell-ECM adhesion is extremely strong, we found cell movement was almost completely eliminated, which reproduces the experimental findings of Riccalton-Banks (2002) for cells seeded on tissue culture plastic. On the basis of these results, we predict that reducing the strength of cell-substrate adhesion may promote the formation of large aggregates. In practice, some degree of cell-substrate adhesion may be necessary for cell locomotion, which would make the elimination of this effect undesirable.

In our model, the properties of the ECM (i.e., its viscosity and elastic modulus) do not have a significant effect on cell aggregation. This suggests any effect of changing the ECM's mechanical properties must come about through an ECM-modulated change in cell behavior, e.g., the strength of cell-ECM adhesion (characterized by the parameter k_2). This hypothesis could be further investigated experimentally. Evidence already exists that some cell types form weaker adhesions to compliant substrates (Gracheva and Othmer, 2004), suggesting a more complex relation between the physical properties of the ECM and the strength of cell-ECM adhesion than has been assumed here. We could extend our model by replacing the parameter k_2 with a more complex function involving μ_E and E'. However, although the current experimental literature contains a number of studies of spheroid formation on a variety of substrates, the mechanical properties of the substrates are not well characterized. We would suggest that further experimental investigation of the impact of the material properties of the substrate on cell adhesion may prove fruitful, and might allow us to postulate the form of a function to replace k_2. Furthermore, our use of a drag term to model cell adhesion is also an idealization of the biological situation. An alternative approach has been taken by Preziosi and Astanin (2005), who when modeling the formation of capillaries, distinguished between a "viscous" cell-ECM interaction force (equivalent to our cell-ECM drag term) and an "elastic" force, which

acts if the cells have had sufficient time to anchor to the ECM (or alternatively, if cells are moving sufficiently slowly), and is proportional to their relative displacement. We also remark that cell motility may depend on ECM properties, as a recent model of cell crawling (Thomas and DiMilla, 2000) suggests that cells move with maximum speed on rigid substrates: on compliant materials the ECM may deform preferentially relative to the cell, retarding cell motion. We could incorporate this effect by making the function Σ_n dependent upon ρ and the ECM's mechanical properties.

Our simulations and analytical work suggest that the cell seeding density plays an important role in aggregate formation. In Section 3, we showed that if the cells are seeded too densely (i.e., $n > n_c$), then aggregation will not occur. Our numerical results also suggest that reducing the cell seeding density leads to the formation of smaller aggregates. This agrees with experimental observations reported by Tong et al. (1994). We thus believe it would be profitable to undertake a quantitative experimental study of the relationship between cell seeding density and spheroid size to see if these predictions can be confirmed. Taken together with the findings above, this result suggests that the most favorable conditions for the formation of large-scale aggregates are high (but not too high) cell seeding density, and low cell-ECM and cell-culture medium drag.

The most obvious weakness of our model is the *ad hoc* adoption of a one-dimensional geometry. Furthermore, although we have not considered chemical signaling explicitly, aggregation is almost certainly influenced by chemical factors. For example, when hepatocyte conditioned medium (culture medium in which hepatocytes have previously been grown) is added to freshly isolated cells, their rate of aggregation increases (Fujii et al., 2000). This suggests that the hepatocytes produce a chemical signal which enhances their motility. Moreover, hepatocytes are known to respond chemotactically to hepatocyte growth factor (HGF) and epidermal growth factor (EGF) *in vitro* (Stolz and Michalopoulos, 1997). Extending our model to investigate the impact of chemical signaling on cell aggregation would require us to augment our system of equations with an expression describing the production and diffusion of the chemical species and incorporate dependence upon the chemical concentration into the function Σ_n (Byrne and Owen, 2004). As a first step toward addressing these points, a two-dimensional version of the model (representing a vertical slice through the culture well), which also includes chemotaxis, has been developed by Green (2006). Thin-film approximations are then used to obtain one-dimensional systems of governing equations in two scaling regimes.

Alternatively, by extending our model to allow for multiple cell populations, we could investigate the impact of cellular heterogeneity on the rate of aggregation and the size of aggregates formed. Recent experimental research has looked at the effect of coculturing hepatocytes with other cell types, such as hepatic stellate cells (Riccalton-Banks et al., 2003), fibroblasts (Bhandari et al., 1997) and pancreatic islet cells (Lee et al., 2004). Under such conditions, spheroids appear to form more quickly, and may also be larger than those which arise in hepatocyte-only cultures. These cell types could easily be included as an additional phase within our multiphase framework.

In conclusion, this paper represents a first attempt to use mathematics to gain insights into the dynamics of spheroid formation, and our model predictions show good qualitative agreement with independent experimental results. In the absence of relevant experimental data, we were forced to make several modeling assumptions concerning, in particular, the nature of cell-substrate interactions and the constitutive law which describes the cells.

While we believe the form chosen for Σ_n is consistent with the type of interactions required to form aggregates of bounded cell density, other choices with the same qualitative behavior (i.e., that the function is unbounded and positive as $n \to 1$, and has only one stationary point and one zero) might equally well have been considered. Extensions to the model, and careful validation against experimental results will be needed if our predictions are to be made quantitatively accurate. However, an advantage of our general model framework is that it can easily be extended or modified to take into account more complex experimental situations, as described above.

Acknowledgements

We would like to thank Dr. Rena Bhandari and Mr. Robert Thomas for helpful discussions, and Dr. Lisa Riccalton-Banks for providing Fig. 1. We are also grateful to Dr. Andrew Grief and Dr. James Oliver for assistance with the numerical simulations. JEFG was supported by a BBSRC studentship and SLW, KMS, and HMB by EPSRC Advanced Fellowships.

Appendix A: Weakly nonlinear analysis

In this Appendix, we undertake a weakly nonlinear analysis (Maini and Murray, 1988) of the 1D model developed in Section 2.1, and construct approximate solutions to the governing equations when the system is close to marginal stability. To perform this analysis, we introduce an additional diffusion term (with coefficient D) on the RHS of Eq. (19) which stabilizes the highest wavenumber modes; without it, standard techniques cannot be applied, as there are an infinite number of unstable modes. (We justify the inclusion of a diffusion term on the basis that it describes more realistically the behavior of the cells, which will undergo a small amount of random motion, and that it replicates the numerical method used in Section 5.) We focus on the limit $\hat{k}_2 = 0$ in which cell-ECM adhesion is negligible, as this simplifies the analysis considerably. The equations under consideration are thus

$$\frac{\partial n}{\partial t} + \frac{\partial}{\partial x}(n v_n) = D\frac{\partial^2 n}{\partial x^2}, \tag{A.1}$$

$$\kappa(n) v_n + \frac{\partial}{\partial x}\big(n\Sigma_n(n)\big) - \frac{\partial}{\partial x}\left(n\frac{\partial v_n}{\partial x}\right) = 0. \tag{A.2}$$

In (A.2), we have left the additional pressure term Σ_n in general form, and introduced $\kappa(n)$ as a general form of the cell-culture medium drag term. (For the choice of drag coefficient specified in Section 2.2, we would have $\kappa(n) = \hat{k}_1 n/(1-n)$.) We solve (A.1)–(A.2) subject to the boundary conditions:

$$v_n = 0, \qquad \frac{\partial n}{\partial x} = 0 \quad \text{at } x = 0, \frac{1}{\epsilon}. \tag{A.3}$$

We now repeat the linear stability analysis of Section 3 for Eqs. (A.1) and (A.2). We consider small-amplitude perturbations to the spatially homogeneous steady state of the form:

$$n = n_0 + \hat{n}e^{iqx+\omega t}, \qquad v_n = \hat{v}_n e^{iqx+\omega t}, \tag{A.4}$$

where q and ω are, respectively, the wavenumber and growth rate of the perturbation and $|\hat{n}|, |\hat{v}_n| \ll 1$. Substituting (A.4) into Eqs. (A.1) and (A.2) yields

$$\omega = -q^2\left(D + \frac{n_0\Lambda'(n_0)}{(\kappa(n_0) + n_0q^2)}\right), \tag{A.5}$$

where $\Lambda(n) = n\Sigma_n$ and a prime denotes differentiation. We hence note that for instability to occur, we require:

$$\Lambda'(n_0) < \frac{-D(\kappa(n_0) + n_0q^2)}{n_0}. \tag{A.6}$$

The addition of the diffusion term is stabilizing, as we would expect, since in the limit $D \to 0$, we require $\Lambda'(n_0) < 0$ (or equivalently $\beta < 0$ in the notation of Section 3).

We note from (A.5) that if

$$D + \frac{n_0\Lambda'(n_0)}{(\kappa(n_0) + n_0q^2)} = 0, \tag{A.7}$$

then $\omega = 0$ (i.e., the growth rate is undetermined at leading order). Condition (A.7) can be viewed as specifying a critical wavenumber, q, given fixed values of n_0 and D. Alternatively, (A.7) may be used to determine critical parameter values for which a given wavenumber q has $w(q) = 0$. We note further that in order to satisfy the boundary conditions at $x = 0, 1/\epsilon$, we require that the additional condition $q = m\pi\epsilon$ (where m is an integer) must hold. In fact, it is necessary to assume the stronger constraint $m = 1$, as for $m > 1$, there exists a smaller permissible wavenumber, for which $\mathcal{R}(\omega) > 0$. We would then expect this longer-wavelength mode to dominate.

To determine the growth rate, we rescale the governing equations on a longer timescale. We introduce a small parameter, $0 < \delta \ll 1$, and adopt a long timescale $t = \delta^{-2}T$. Equation (A.2) is unchanged as a result of this rescaling, while (A.1) becomes

$$\delta^2\frac{\partial n}{\partial T} + \frac{\partial}{\partial x}(nv_n) = D\frac{\partial^2 n}{\partial x^2}. \tag{A.8}$$

We seek solutions of the form:

$$n = n_0 + \delta n_1(x,T) + \delta^2 n_2(x,T) + \cdots, \qquad v_n = \delta v_1(x,T) + \delta^2 v_2(x,T) + \cdots, \tag{A.9}$$

and also write $D = D_0 + \delta^2 D_1 + \cdots$, where D_0 is the value of D satisfying (A.7), i.e.,

$$D_0 = -\frac{n_0\Lambda'(n_0)}{(\kappa(n_0) + n_0q^2)}. \tag{A.10}$$

At $O(\delta)$, Eqs. (A.8) and (A.2) give

$$n_0 \frac{\partial v_1}{\partial x} = D_0 \frac{\partial^2 n_1}{\partial x^2}, \tag{A.11}$$

$$n_0 \frac{\partial^2 v_1}{\partial x^2} = \left(\kappa(n_0) + \frac{n_0 \Lambda'}{D_0}\right) v_1. \tag{A.12}$$

Solving the above subject to the boundary conditions yields, and using (A.7) gives

$$n_1 = -\left(\frac{n_0}{D_0 q}\right) A(T) \cos qx, \qquad v_1 = A(T) \sin qx, \tag{A.13}$$

where $q = \pi\epsilon$ and $A(T)$ is the amplitude of velocity (which is also related to the amplitude of n_1), which is determined at $O(\delta^3)$.

Continuing to next order, we find

$$n_0 \frac{\partial v_2}{\partial x} + \frac{\partial}{\partial x}(n_1 v_1) = D_0 \frac{\partial^2 n_2}{\partial x^2}, \tag{A.14}$$

$$\kappa(n_0) v_2 + \kappa'(n_0) n_1 v_1 + \Lambda'(n_0) \frac{\partial n_2}{\partial x} + \Lambda''(n_0) n_1 \frac{\partial n_1}{\partial x}$$
$$- n_0 \frac{\partial^2 v_2}{\partial x^2} - \frac{\partial}{\partial x}\left(n_1 \frac{\partial v_1}{\partial x}\right) = 0. \tag{A.15}$$

We seek solutions of the form:

$$n_2 = N_2 A^2(T) \cos(2qx), \qquad v_2 = V_2 A^2(T) \sin(2qx), \tag{A.16}$$

where N_2 and V_2 are constants. Substituting these forms into Eqs. (A.14) and (A.15) yields

$$N_2 = \frac{n_0}{(2D_0 q)^2}\left[1 - \left(\frac{1}{3q^2}\left(\frac{\Lambda'(n_0)}{D_0} + \kappa'(n_0)\right) + \frac{2}{3} + \frac{n_0 \Lambda''(n_0)}{3D_0 q^2}\right)\right], \tag{A.17}$$

$$V_2 = \frac{1}{6D_0 q^3}\left(\kappa'(n_0) + \frac{\Lambda'(n_0)}{D_0}\right) + \frac{1}{3D_0 q} + \frac{n_0 \Lambda''(n_0)}{6D_0^2 q^3}. \tag{A.18}$$

At $O(\delta^3)$, we have

$$\frac{\partial n_1}{\partial T} + \frac{\partial}{\partial x}(n_1 v_2 + n_2 v_1) + n_0 \frac{\partial v_3}{\partial x} = D_0 \frac{\partial^2 n_3}{\partial x^2} + D_1 \frac{\partial^2 n_1}{\partial x^2}, \tag{A.19}$$

$$\kappa(n_0) v_3 + \kappa'(n_0)(n_1 v_2 + n_2 v_1) + \frac{\kappa''(n_0)}{2} n_1^2 v_1 + \Lambda'(n_0) \frac{\partial n_3}{\partial x} + \Lambda''(n_0) \frac{\partial}{\partial x}(n_1 n_2)$$
$$+ \frac{\Lambda'''(n_0) n_1^2}{2} \frac{\partial n_1}{\partial x} - n_0 \frac{\partial^2 v_3}{\partial x^2} - \frac{\partial}{\partial x}\left(n_1 \frac{\partial v_2}{\partial x} + n_2 \frac{\partial v_1}{\partial x}\right) = 0. \tag{A.20}$$

In order to suppress the resonant terms, we require

$$-\frac{\kappa'(n_0) A^3}{2}\left(N_2 + \frac{n_0 V_2}{D_0 q}\right) + \frac{\kappa''(n_0) A^3}{8}\left(\frac{n_0}{D_0 q}\right)^2 + \frac{q^2 A^3}{2}\left(N_2 - \frac{2n_0 V_2}{D_0 q}\right)$$

$$-\frac{\Lambda'(n_0)}{D_0}\left[\left(\frac{n_0}{D_0q^2}\right)\left(\frac{dA}{dT}+q^2D_1A\right)+\frac{A^3}{2}\left(N_2+\frac{n_0V_2}{D_0q}\right)\right]$$
$$+\frac{q\Lambda''(n_0)N_2}{2}\left(\frac{n_0}{D_0q}\right)A^3+\frac{q\Lambda'''(n_0)}{8}\left(\frac{n_0}{D_0q}\right)^3A^3=0. \tag{A.21}$$

The above hence reduces to the Landau equation (Maini and Murray, 1988)

$$\frac{dA}{dt}=\alpha_1A+\alpha_2A^3, \tag{A.22}$$

where the coefficients are given by

$$\alpha_1=-q^2D_1, \tag{A.23}$$
$$\alpha_2=\frac{q^2D_0^2}{n_0\Lambda'(n_0)}\left[\frac{-\kappa'(n_0)}{2}\left(N_2+\frac{n_0V_2}{D_0q}\right)+\frac{\kappa''(n_0)}{8}\left(\frac{n_0}{D_0q}\right)^2+\frac{q^2}{2}\left(N_2-\frac{2n_0V_2}{D_0q}\right)\right.$$
$$\left.-\frac{\Lambda'(n_0)}{2D_0}\left(N_2+\frac{n_0V_2}{D_0q}\right)+\frac{q\Lambda''(n_0)N_2}{2}\left(\frac{n_0}{D_0q}\right)+\frac{q\Lambda'''(n_0)}{8}\left(\frac{n_0}{D_0q}\right)^3\right], \tag{A.24}$$

and, D_0 is related to Λ', q, and κ by Eq. (A.10).

The long-time behavior of the amplitude equation is thus:

(i) For $D_1>0$ and $\alpha_2>0$, $A\to 0$ if $A(0)<\sqrt{(|\alpha_1|/\alpha_2)}$; $A\to\infty$ if $A(0)>\sqrt{(|\alpha_1|/\alpha_2)}$.
(ii) For $\alpha_2<0<D_1$, $A\to 0$.
(iii) For $D_1<0<\alpha_2$, $A\to\infty$.
(iv) For $D_1<0$ and $\alpha_2<0$, $A\to\sqrt{(\alpha_1/|\alpha_2|)}$.

A sketch illustrating how the system dynamics vary in different regions of (D,n_0) parameter space is presented in Fig. A.1, with $q=0.1\pi$, $\kappa(n_0)=n_0/(1-n_0)$ and $\Lambda(n_0)=n_0(n_0-0.8)/(1-n_0)^2$ (these are equivalent to the dimensionless functions used in Section 2.6 with $\hat{k}_1=1$ and $n^*=0.8$). The space is divided up by the curves $\alpha_1=0$ (i.e., $D=D_0$), and those across which $\alpha_2(n_0)$ changes sign; the latter are vertical lines occurring at $n_0=n_\alpha\approx 0.5$ (corresponding to a root of $\alpha_2(n_0)=0$) and $n_0=n_c=2/3$, where n_c is as defined in Section 3 (corresponding to a discontinuity across which α_2 changes sign, since $D_0(n_c)=\Lambda'(n_c)=0$). The behavior of α_2 is quite sensitive to the choice of n^*, e.g., for $n^*=0.9$, there is an additional root of $\alpha_2=0$ for $n<n_c$. (Note that owing to the assumption that $D=D_0+\delta^2D_1$, the predictions of the analysis are only valid for choices of D close to the $\alpha_1=0$ curve.)

Numerical simulations of the governing PDEs in the relevant region of parameter space confirms the predictions of the weakly nonlinear analysis (results not shown). The analysis presented above is valid for a finite interval and breaks down on an infinite domain. In this case, variation of the dependent variables on the long lengthscale (i.e., much longer than the critical wavelength) must be included, together with the potential for mode interaction (Matthews and Cox, 2000).

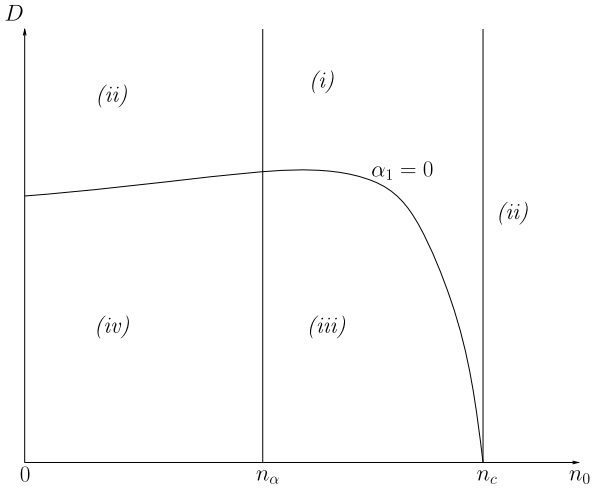

Fig. A.1 Behavior of solutions in different regions of (D, n_0) parameter space (with $q = 0.1\pi$, $\kappa(n_0) = n_0/(1-n_0)$ and $\Lambda(n_0) = n_0(n_0 - 0.8)/(1-n_0)^2$). Labels (i)–(iv) refer to the regimes described in the main text. Note that n_α and n_c are the values of n_0 across which α_2 changes sign (see main text for details). For the given parameter values, $n_\alpha \approx 0.5$, and $n_c = 2/3$ (see Section 3).

References

Abu-Absi, S.F., Friend, J.R., Hansen, L.K., Hu, W.S., 2002. Structural polarity and functional bile canaliculi in rat hepatocyte spheroids. Exp. Cell Res. 274, 56–67.

Babak, P., Magnusson, K.G., Sigurdsson, S., 2004. Dynamics of group formation in collective motion of organisms. Math. Med. Biol. 21, 269–292.

Bedossa, P., Paradis, V., 2003. Liver extracellular matrix in health and disease. J. Pathol. 200, 504–515.

Bhandari, R.N., Riccalton, L.A., Lewis, A.L., Fry, J.R., Hammond, A.H., Tendler, S.J.B., Shakesheff, K.M., 1997. Liver tissue engineering: A role for co-culture systems in modifying hepatocyte function and viability. Tissue Eng. 7, 345–357.

Breward, C.J.W., Byrne, H.M., Lewis, C.E., 2002. The role of cell-cell interactions in a two-phase model for avascular tumour growth. J. Math. Biol. 45(2), 125–152.

Byrne, H.M., Chaplain, M.A.J., 1996. The importance of constitutive equations in mechanochemical models of pattern formation. Appl. Math. Lett. 9(6), 85–90.

Byrne, H.M., Owen, M.R., 2004. A new interpretation of the Keller–Segel model based on multiphase modelling. J. Math. Biol. 49(6), 604–626.

Byrne, H.M., Preziosi, L., 2003. Modelling solid tumour growth using the theory of mixtures. Math. Med. Biol. 20, 341–366.

Centers for Disease Control and Prevention, 2003. Compressed Mortality File (CDC WONDER On-line Database. http://wonder.cdc.gov), Accessed 12 May 2003

Chen, C., Chueh, J., Tseng, H., Huang, H., Lee, S., 2003. Preparation and characterisation of biodegradable PLA polymeric blends. Biomaterials 24, 1167–1173.

Drew, D.A., 1983. Mathematical modelling of two-phase flow. Annu. Rev. Fluid Mech. 15, 261–291.

Drew, D.A., Segel, L.A., 1971. Averaged equations for two-phase flows. Stud. Appl. Math. 3, 205–231.

Enat, R., Jefferson, D.M., Ruiz-Opazo, N., Gatmaitian, Z., Leinwand, L.A., Reid, L.M., 1984. Hepatocyte proliferation *in vitro*: Its dependence on the use of serum-free hormonally defined medium and substrata of extracellular matrix. Proc. Natl. Acad. Sci. USA 81, 1411–1415.

Forgacs, G., Foty, R.A., Shafrir, Y., Steinberg, M.S., 1998. Viscoelastic properties of living embryonic tissues: A quantitative study. Biophys. J. 74, 2227–2234.

Fujii, Y., Nakazawa, K., Funatsu, K., 2000. Intensive promotion of spheroid formation by soluble factors in a hepatocyte-conditioned medium. J. Biomater. Sci. Polym. Ed. 11(7), 731–745.

Glicklis, R., Shapiro, L., Agbaria, R., Merchuk, J.C., Cohen, S., 2000. Hepatocyte behaviour within three-dimensional porous alginate scaffolds. Biotechnol. Bioeng. 67(3), 344–353.
Glicklis, R., Merchuk, J.C., Cohen, S., 2004. Modelling mass transfer in hepatocyte spheroids via cell viability, spheroid size and hepatocellular functions. Biotechnol. Bioeng. 86(6), 672–680.
Gracheva, M.E., Othmer, H.G., 2004. A continuum model of motility in ameboid cells. Bull. Math. Biol. 66, 167–193.
Green, J.E.F., 2006. Mathematical modelling of cell aggregation in liver tissue engineering. Ph.D. thesis, University of Nottingham, UK.
Gunatillake, P.A., Adhikari, R., 2003. Biodegradable synthetic polymers for tissue engineering. Eur. Cell. Mater. 5, 1–16.
Higuchi, A., Tsukamoto, Y., 2004. Cell separation of hepatocytes and fibroblasts through surface-modified polyurethane membranes. J. Biomed. Mater. Res. Part A 71A: (3), 470–479.
Jackson, T.L., Byrne, H.M., 2002. A mechanical model of tumour encapsulation and transcapsular spread. Math. Biosci. 180, 307–328.
Jauregui, H.O., 2000. Principles of Tissue Engineering, 2nd edn. Liver, Academic, New York, Chap. 39, pp. 541–551.
Keller, E.F., Segel, L.A., 1970. Initiation of slime mold aggregation viewed as an instability. J. Theor. Biol. 26, 399–415.
Keller, E.F., Segel, L.A., 1971. Model for chemotaxis. J. Theor. Biol. 30, 225–234.
Kowalczyk, R., Gamba, A., Preziosi, L., 2004. On the stability of homogeneous solutions to some aggregation models. Discrete Contin. Dyn. Syst. B 4(1), 203–220.
Lee, K.W., Lee, S.K., Joh, J.W., Kim, S.J., Lee, B.B., Kim, K.W., Lee, K.U., 2004. Influence of pancreatic islets on spheroid formation and functions of hepatocytes in hepatocyte-pancreatic islet spheroid culture. Tissue Eng. 10, 965–977.
Lemon, G., King, J.R., Byrne, H.M., Jensen, O.E., Shakesheff, K.M., 2006. Mathematical modelling of engineered tissue growth using a multiphase porous flow mixture theory. J. Math. Biol. 52, 571–594.
Lubkin, S.R., Jackson, T., 2002. Multiphase mechanics of capsule formation in tumours. J. Biomech. Eng. 124, 237–243.
Maini, P.K., Murray, J.D., 1988. A nonlinear analysis of a mechanical model for biological pattern formation. SIAM J. Appl. Math. 48(5), 1064–1072.
Matthews, P.C., Cox, S.M., 2000. Pattern formation with a conservation law. Nonlinearity 13(4), 1293–1320.
Mitaka, T., 1998. The current status of primary hepatocyte culture. Int. J. Exp. Pathol. 79, 393–409.
Moghe, P.V., Berthiaume, F., Ezzell, R.M., Toner, M., Tompkins, R.G., Yarmush, M.L., 1996. Culture matrix configuration and composition in the maintenance of hepatocyte polarity and function. Biomaterials 17, 373–385.
Moghe, P.V., Coger, R.N., Toner, M., Yarmush, M.L., 1997. Cell-cell interactions are essential for maintenance of hepatocyte function in collagen gel but not on matrigel. Biotechnol. Bioeng. 56(6), 706–710.
Murray, J.D., 1993. Mathematical Biology, 2nd edn. Springer, New York.
Namy, P., Ohayon, J., Tracqui, P., 2004. Critical conditions for pattern formation and *in vitro* tubulogenesis driven by cellular traction fields. J. Theor. Biol. 227, 103–120.
NHS, 2001. Liver activity. UK transplant activity 2001, UK Transplant—NHS.
Oliver, J.M., King, J.R., McKinlay, K.J., Grant, D.M., Scotchford, C.A., Wood, J.V., Brown, P.D., 2005. Thin film theories for two-phase reactive flow models of active cell motion. Math. Med. Biol. 22, 53–98.
OPTN, 2003. Donors and waiting list 1993–2003. Organ Procurement and Transplantation Network. www.optn.org. Accessed 16 Sept. 2003.
Owen, M.R., Byrne, H.M., Lewis, C.E., 2004. Mathematical modelling of the use of macrophages as vehicles for drug-delivery to hypoxic tumour sites. J. Theor. Biol. 226, 377–391.
Peshwa, M.V., Wu, F.J., Follstad, B.D., Cerra, F.B., Hu, W., 1994. Kinetics of hepatocyte spheroid formation. Biotechnol. Prog. 10, 460–466.
Peshwa, M.V., Wu, F.J., Sharp, H.L., Cerra, F.B., Hu, W., 1996. Mechanistics of formation and ultrastructural evaluation of hepatocyte spheroids. In Vitro Cell Dev. Biol. 32, 197–203.
Powers, M.J., Griffith-Cima, L., 1996. Motility behaviour of hepatocytes on extracellular matrix substrata during aggregation. Biotechnol. Bioeng. 50, 392–403.
Powers, M.J., Rodriguez, R.E., Griffith, L.G., 1997. Cell-substratum adhesion strength as a determinant of hepatocyte aggregate morphology. Biotechnol. Bioeng. 53, 415–426.

Powers, M.J., Domansky, K., Kaazempur-Mofrad, M.R., Kalezi, A., Capitano, A., Upadhyaya, A., Kurzawski, P., Wacka, K.E., Stolz, D.B., Kamm, R., Griffith, L.G., 2002. A microfabricated array bioreactor for perfused 3D liver cultures. Biotechnol. Bioeng. 78(3), 257–269.

Preziosi, L., Astanin, S., 2005. Modelling the formation of capillaries. In: Quarteroni, A. (Ed.), Integration of Complex Systems in Biomedicine. Springer, New York. Chap. 4.

Riccalton-Banks, L., Liew, C., Bhandari, R., Fry, J., Shakesheff, K., 2003. Long-term culture of functional liver tissue: Three-dimensional coculture of primary hepatocytes and stellate cells. Tissue Eng. 9(3), 401–409.

Riccalton-Banks, L.A., 2002. Maintenance of primary rat hepatocytes *in vitro* using co-culture techniques. Ph.D. thesis, University of Nottingham.

Richert, L., Binda, D., Hamilton, G., Viollon-Abadie, C., Alexandre, E., Bigot-Lasserre, D., Bars, R., Coassolo, P., LeCluyse, E., 2002. Evaluation of the effect of culture configuration on morphology, survival time, antioxidant status and metabolic capacities of cultured rat hepatocytes. Toxicol. In Vitro 16, 89–99.

Selden, C., Khalil, M., Hodgson, H.J.F., 1999. What keeps hepatocytes on the straight and narrow? Maintaining differentiated liver function. Gut 44, 443–446.

Stolz, D.B., Michalopoulos, G.K., 1997. Synergistic enhancement of EGF, but not HGF, stimulated hepatocyte motility by TGF-β1 *in vitro*. J. Cell. Physiol. 170, 57–68.

Strikwerda, J.C., 1989. Finite Difference Schemes and Partial Differential Equations. Wadsworth and Brooks/Cole Advanced Books and Software, Belmont.

Swabb, E.A., Wei, J., Gullino, P.M., 1974. Diffusion and convection in normal and neoplastic tissues. Cancer Res. 34, 2814–2822.

Thomas, R.J., Bhandari, R., Barrett, D.A., Bennett, A.J., Fry, J.R., Powe, D., Thomson, B.J., Shakesheff, K.M., 2005. The effect of three-dimensional co-culture of hepatocytes and hepatic stellate cells on key hepatocyte functions *in vitro*. Cells Tissues Organs 181, 67–79.

Thomas, R.J., Bennett, A., Thomson, B., Shakesheff, K.M., 2006. Hepatic stellate cells on poly(DL-lactic acid) surfaces control the formation of 3D hepatocyte co-culture aggregates *in vitro*. Eur. Cell. Mater. 11, 16–26.

Thomas, T.W., DiMilla, P.A., 2000. Spreading and motility of human gliobastoma cells on sheets of silicone rubber depend on substratum compliance. Med. Biol. Eng. Comput. 38, 360–370.

Tong, J.Z., Sarrazin, S., Cassio, D., Gaulthier, F., Alvarez, F., 1994. Application of spheroid culture to human hepatocytes and maintainance of their differentiation. Biol. Cell 81, 77–81.

Vasiev, B., Weijer, C.J., 2003. Modelling of Dictyostelium discoideum slug migration. J. Theor. Biol. 223, 347–359.

Velegol, D., Lanni, F., 2001. Cell traction forces on soft biomaterials. I Microrheology of type I collagen gels. Biophys. J. 81, 1786–1792.

Whitaker, M.J., 2003. Supercritical fluid processing of polymers, proteins and cells for tissue engineering applications. Ph.D. thesis, University of Nottingham.